Large-Signal Photomagnetoelectric Effect

ALAN R. BEATTIE AND R. W. CUNNINGHAM
Texas Instruments Incorporated, Dallas, Texas
(Received August 22, 1961)

Photomagnetoelectric measurements made on p-type InSb at 80°K are found to disagree with existing theories. The theory is extended to include nonlinear bulk and surface recombination rates which define a "lifetime", $\tau_n(\Delta n)$, and a "surface recombination velocity", $S_n(\Delta n)$, which are dependent on excess carrier concentration. This extended theory is in good agreement with experiment, and is used to determine $\tau_n(\Delta n)$ and $S_n(\Delta n)$ as functions of Δn, to determine the zero-magnetic-field mobility of the minority carrier, and to identify the dominant scattering mechanism. Agreement between theory and experiment is best when ionized impurity type scattering is assumed, yielding a zero-magnetic-field electron mobility of 1.1×10^5 cm²/v-sec. The "lifetime" begins to deviate from its small signal value (1.6×10^{-10} sec) when Δn exceeds about 10^9 cm^{-3}; it increases by a factor of 20 as Δn increases to 5×10^{10} cm^{-3}. The small-signal "surface recombination velocity" is too small to be determined. It becomes appreciable (the order of 3.5×10^4 cm/sec) when Δn is about 10^9 cm^{-3}, increases rapidly to a maximum of 12×10^4 cm/sec when Δn is 3.8×10^9 cm^{-3}, and then falls off gradually by a factor of 1.5 when Δn reaches 2×10^{10} cm^{-3}.

I. INTRODUCTION

THE photomagnetoelectric (PME) effect has been used to study excess minority carrier transport in p-type InSb at 80°K. When a semiconductor in a magnetic field has a surface illuminated such that a carrier concentration gradient is produced perpendicular to the field, charge separation occurs. This effect may be observed as a short-circuit current (subsequently called s-c current) in the third mutually perpendicular direction, as shown in Fig. 1.

Previous theories of the PME effect[1–6] have proved satisfactory for many applications, for instance in the case of InSb at room temperature. However, the experimental results which we observe in InSb near liquid nitrogen temperature do not display the strict proportionality of short-circuit current with photon flux which is predicted by these theories. Such nonlinearity has also been observed by Zitter, *et al.*[7] Figure 2 shows typical results of s-c current as a function of photon flux for constant magnetic field.

Kurnick and Zitter[1] have suggested that the mobility and diffusion length can be obtained from the magnetic field dependence of the PME effect. A graph of $(B\phi/i_{sc})^2$ vs B^2 (the symbols used throughout this paper are defined in Table I) should be independent of photon flux, and will be a straight line if the electron relaxation time is energy independent. A typical graph for one of our samples is shown in Fig. 3. The bending near the origin, shown as an insert in Fig. 3, indicates an energy-dependent relaxation time,[1] but the dependence on photon flux precludes the use of previous theories to analyze the results.

Common to all previous calculations is the assumption that the thermal equilibrium concentrations of carriers p_0, n_0 are much greater than their corresponding excess concentrations Δp, Δn so that the recombination rate R, is proportional to Δn. For the p-type material used p_0 is approximately 10^{14} cm^{-3} and n_0 is approximately 10^5 cm^{-3} at 80°K. For an applied photon flux of about 10^{15} cm^{-2} sec^{-1}, Δn is of the order 10^9 cm^{-3}, when previously reported[5,7] values of lifetime and mobility are assumed. Since Δn is much greater than n_0, R may not be linear with Δn so that a concentration-dependent "lifetime", $\tau_n(\Delta n)$, defined by $R=\Delta n/\tau_n(\Delta n)$ is introduced. An analogous definition holds for a concentration-dependent surface recombination velocity $S_n(\Delta n)$.

This paper gives the results of an experimental and theoretical study of the PME effect in p-type InSb at 80°K. The experimental apparatus and techniques are described and a two-carrier theory applicable to nondegenerate extrinsic material is developed. Analysis of the experimental data with this theory gives self-consistent values for the electron lifetime and surface recombination velocity as functions of excess electron concentration. The dominant scattering mechanism is also identified and the electron mobility is found.

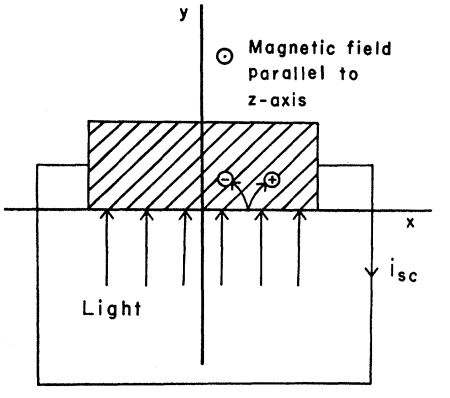

FIG. 1. Schematic representation of the PME effect.

[1] S. W. Kurnick and R. N. Zitter, J. Appl. Phys. **27**, 278 (1956).
[2] W. van Roosbroeck, Phys. Rev. **101**, 1713 (1956).
[3] T. S. Moss and T. H. Hawkins, Phys. Rev. **101**, 1609 (1956).
[4] L. Pincherle, *Proceedings of the Photoconductivity Conference, Atlantic City, 1954* (John Wiley & Sons, Inc., New York, 1956), p. 307 ff.
[5] R. A. Laff and H. Y. Fan, Phys. Rev. **121**, 53 (1961).
[6] A. K. Walton and T. S. Moss, Proc. Phys. Soc. (London) **73**, 399 (1959).
[7] R. N. Zitter, A. J. Strauss, and A. E. Attard, Phys. Rev. **115**, 266 (1959).

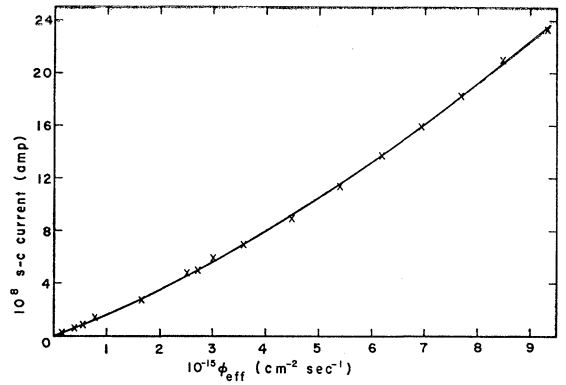

FIG. 2. Total s-c current vs effective photon flux ϕ_{eff}, for constant magnetic field ($B=0.08$ weber/m^2).

II. EXPERIMENTAL PROCEDURE

Although the experimental procedure used in this work is similar to that used by others,[1,7] there are important variations in equipment and technique. A schematic diagram of the apparatus is given in Fig. 4. There are three main sections to the apparatus: (1) photon source, (2) magnet system, and (3) measuring system.

Our photon source is a high-intensity tungsten filament lamp with an internal reflector focused on an aperture. An image of the aperture is focused at a point behind the sample by the front surfaced plane and spherical mirrors so that the photon flux was uniform over a sample width. The light is rendered nearly monochromatic by a Corning Glass 7-85 narrow-band filter whose pass band is peaked at 0.94 μ. The absolute photon flux was obtained from the measured filter transmission and the output of a calibrated radiation thermocouple placed at the sample position. The light intensity may be attenuated by calibrated screens placed near the aperture, or by the attenuator.[8] The screens and attenuator were calibrated so that the relative transmission of each step was accurate to within $\pm 1\%$. The light was modulated sinusoidally at 570 cps by a 19-slot rotating disk. This frequency, was chosen because it has little interference from 60-cps noise. The photon flux was set to a given value before each series of measurements and monitored continuously during measurements to maintain a constant intensity.

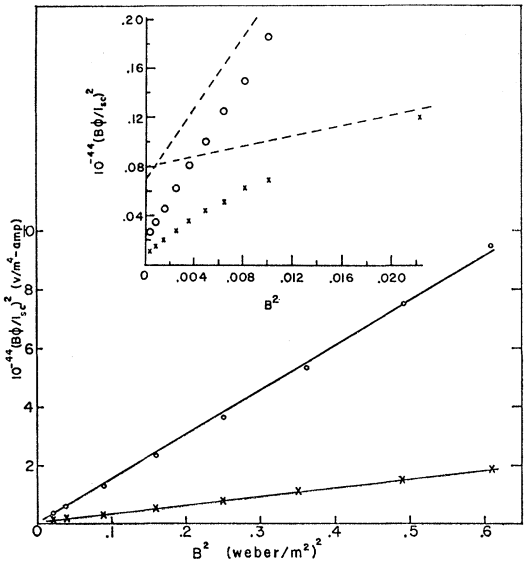

FIG. 3. Typical magnetic field dependences of PME data for p-type InSb at 80°K at two different photon fluxes, displayed by plotting $(B\phi/i_{sc})^2$ vs B^2. If small-signal theory were applicable, the crosses and circles would be coincident. The insert shows the portion of the curves near the origin, where the dashed lines are a linear extrapolation of the straight lines of the larger range.

Table I—List of Symbols

$\mathbf{B}$	Magnetic induction
b	μ_0/μ_{0h}
b_1	μ_1/μ_{1h}
D	Zero-magnetic-field electron diffusion constant
e	Electronic charge
$\mathcal{E}$	Electric field
E	Electron energy
$f(\Delta n_0)$	See equation (3.22)
i_{sc}	Short-circuit current per unit sample width
$\mathbf{J}_e$	Electric current density of electrons
$\mathbf{J}_h$	Electric current density of holes
k	Boltzmann's constant
$K(B)$	$[2D\mu_1/\mu_0(1+\mu_0^2B^2)]^{\frac{1}{2}}$ [Eq. (3.21)]
m^*	Electron effective mass
n_0	Thermal equilibrium density of electrons
p_0	Thermal equilibrium density of holes
$r(\Delta n)$	$\Delta p/\Delta n=\tau_p(\Delta p)/\tau_n(\Delta n)$
$r'(\Delta n)$	$d[r(\Delta n)]/d(\Delta n)$
R	Recombination rate
$S_n(\Delta n)$	Electron "surface recombination velocity"
T	Absolute temperature
x	E/kT
γ	$e\tau_{\text{rel}}/m^*$
Δn	Density of excess electrons
Δp	Density of excess holes
Δn_0	Density of excess electrons at the surface
Δp_0	Density of excess holes at the surface
η	Quantum efficiency
μ_0	Zero-magnetic-field electron mobility
μ_{0h}	Zero-magnetic-field hole mobility
μ_1, μ_2	Magnetic-field-dependent electron "mobilities" defined in equations (3.6) and (3.7)
μ_{1h}, μ_{2h}	Hole "mobilities" analogous to μ_1 and μ_2, respectively
$\tau_n(\Delta n)$	Electron "lifetime" given by $\Delta n/R$
$\tau_p(\Delta p)$	Hole "lifetime" given by $\Delta p/R$
τ_{rel}	Electron relaxation time
ϕ	Photon flux

Short-circuit currents were measured because they can be easily compared to theory. The PME currents were determined by a substitution or comparative

[8] J. P. Luongo, Appl. Spectroscopy 14, 24 (1960).

method which avoids instrumental gain calibrations. With the shutter open and magnetic field applied, a PME signal is generated within the sample and amplified by a transformer-amplifier combination. Only the 570-cps component of the signal is measured by a wave analyzer acting as a narrow-band voltmeter. A recorder is used to obtain a permanent record of the signal. The shutter is then closed and a substitution signal obtained from the BFO terminals of the wave analyzer is applied to the ends of the sample through a large series resistance, while the magnetic field remains unchanged. The amplitude of this signal is varied by a microvolter until the PME signal level is reproduced. Analysis of the circuit shows that the PME short circuit current is given by dividing the open circuit voltage of the microvolter by the series resistance. The s-c currents determined in this way had a relative accuracy within $\pm 3\%$, a limit set by the microvolter calibration. PME currents as low as 10^{-11} amp could be observed with this apparatus, although typical values were of the order of 10^{-10} amp or larger. Great care was taken to eliminate ground loops and multiple signal paths.

Magnetic fields up to 7600 gauss (0.76 weber/m^2) were obtained from a Varian four-inch electromagnet. Each field was measured during experiments with a rotating-coil gauss meter whose error was less than $\pm 3\%$. The reproducibility of any field was within $\pm 0.5\%$. Stability of the magnetic field was substantially better than $\pm 0.1\%$ during all the measurements.

The samples were obtained from the p-type ends of single-crystal zone refined bars. Each sample was prepared by standard laboratory techniques, Cavitroned to shape and etched before it was mounted for measurements. The samples were 12 mm$\times$3 mm$\times\approx$1 mm, with side arms separated by 3 mm. Leads were attached to the unilluminated side by Cerroseal 35 solder and the contact areas were masked by brass shields to further

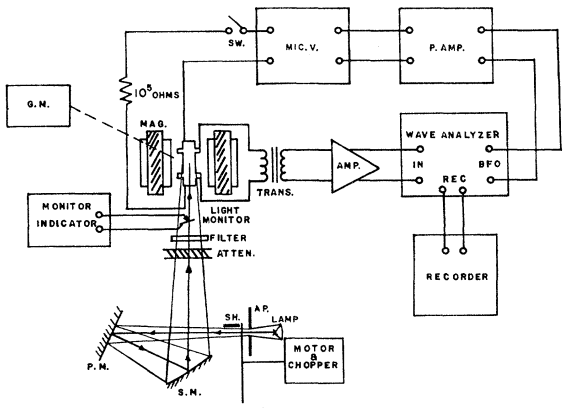

FIG. 4. Schematic diagram of the apparatus. The symbols refer to the following: S.M. spherical mirror; P.M. plane mirror; S.H. shutter; A.P. aperture; ATTEN. optical attenuator; MAG electro-magnet; TRANS. transformer; AMP low noise preamplifier; G.M. gauss meter; P. AMP. power amplifier; MIC. V. microvolter; SW. switch; BFO auxiliary output tuned to input frequency.

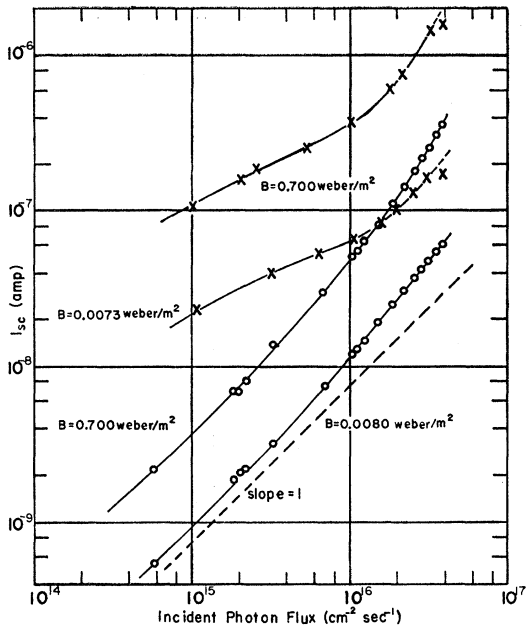

FIG. 5. Total s-c current vs total incident photon flux with and without background. The cross data was taken in the presence of 300°K blackbody background radiation.

insure against unwanted photo signals. The illumination was incident on the (311) plane. The samples were butt-soldered onto a copper plate by heating the sample and copper plate to a temperature just below the solder melting point and adding heat from a small soldering iron to complete the bond. The entire assembly was then allowed to cool slowly. This technique eliminated sample fracture due to thermal strains when a sample was cooled suddenly in liquid nitrogen. Before mounting, the samples were etched in a superoxyl etch described by Zitter *et al.*[7] The etch was found to be irreproducible, not always giving a low surface recombination velocity. However, after suitable adjusting, a low surface recombination velocity could be produced on specific samples.

After the samples were prepared and mounted they were secured to the copper heat sink of a vacuum cryostat. The cryostat had an outer jacket containing a pumping port, a light port covered by a Pyrex window, and an inner chamber containing a liquid coolant reservoir connected to the sample heat sink by a J tube. In these experiments liquid nitrogen was the coolant, so that a sample temperature of approximately 80°K could be maintained for long periods of time. The ambient pressure was maintained at less than 10^{-3} mm Hg.

Early measurements of PME s-c current as a function of photon flux indicated a complicated behavior, shown as crosses in Fig. 5. These curves show both a sublinear and a superlinear region with a fairly sharp break between them. It was suggested[9] that a steady back-

[9] G. R. Pruett (private communication).

ground of 300°K blackbody photons might complicate the shape of the curves. The flux density of photons between 0 and 5.7 μ (the absorption edge of InSb at 80°K) from a 300°K blackbody is approximately 10^{16} cm^{-2} sec^{-1}, approximately the position of the break points in Fig. 5.

In order to reduce the number of steady background photons and to form an isothermal enclosure about the sample a one-fourth inch Pyrex plate cooled to 80°K was placed in front of the sample. This plate reduced the background photons by a factor between 10^3 and 10^4 so that the primary effects of illumination were due to the narrow-band illumination. The experimental results for this arrangement are shown as circles in Fig. 5. The character of the curves is entirely different from the curves obtained when the steady background was present. The effect of the background illumination on the s-c current can be understood on the basis of the theory of Sec. III. All the measurements reported below were carried out with the cooled Pyrex filter so that complicated corrections were not necessary.

The presence of slow surface states complicated the measurements. After cooling the sample, a slow drift in signal was observed. The drift usually became small or zero after an hour or more, and measurements were not carried out until a stable signal was obtained. We believe the effect on our measurements is negligible.

III. THEORY

The restrictions of constant lifetime and surface recombination velocity are removed and a theory more general than that for small signals is developed. Two relationships are found. The first connects the s-c current with magnetic field and the concentration of excess minority carriers at the illuminated surface, and the second relates photon flux, magnetic field, surface recombination velocity, and lifetime to the surface concentration of excess carriers.

The calculation is based on the following assumptions:

1. A two-carrier model.
2. Nondegenerate extrinsic material where $p_0 \gg \Delta p$, Δn, n_0 but n_0 is not necessarily greater than Δn.
3. A semi-infinite block.
4. Magnetic fields not strong enough to produce any quantization effects.
5. Scattering of carriers described by relaxation times which may be energy dependent.
6. Parabolic bands and spherical energy surfaces.
7. Recombination rate R, written in the form $R=\Delta n/\tau_n(\Delta n)$.
8. Excess carrier dependent surface recombination velocity similarly defined.
9. Excess carriers created only at the surface.
10. Nonequilibrium carrier distributions described by quasi-Fermi levels.

The analysis based on these assumptions is applicable when the sample dimensions are sufficiently large, so that edge effects are negligible, and when the carrier diffusion lengths are much smaller than the thickness and much larger than the absorption depth of the incident illumination. It may also be applied to nondegenerate n-type material if n and p are interchanged.

The Boltzmann equation for each carrier is solved[10] by considering the electric and magnetic fields as causing a perturbation on the quasi-equilibrium distribution when the semiconductor is illuminated in the absence of electric and magnetic fields. The coordinate system is shown in Fig. 1 where, for a semi-infinite block, $\mathbf{J}_e$, $\mathbf{J}_h$, Δp, Δn, and $\mathbf{\mathcal{E}}$ vary only in the y direction. When there are no externally applied electric fields only the Dember[11] field, which is due to the different mobilities and lifetimes of electrons and holes, remains in the y direction. The electric field is then

$$\mathbf{\mathcal{E}}=(0,\mathcal{E}_y,0),$$

and the magnetic field is applied in the z direction so that

$$\mathbf{B}=(0,0,B).$$

The electron and hole currents which are obtained by this procedure are

$$(1+\mu_0^2B^2)J_{ex}=-(n_0+\Delta n)e\mu_2^2B\mathcal{E}_y - \mu_0^{-1}\mu_2^2eBDd(\Delta n)/dy, \quad (3.1)$$

$$(1+\mu_0^2B^2)J_{ey}=(n_0+\Delta n)e\mu_1\mathcal{E}_y + e\mu_1\mu_0^{-1}Dd(\Delta n)/dy, \quad (3.2)$$

$$(1+b^{-2}\mu_0^2B^2)J_{hx}=(p_0+\Delta p)e\mu_{2h}^2B\mathcal{E}_y - \mu_0^{-1}\mu_{2h}^2eBDd(\Delta p)/dy, \quad (3.3)$$

$$(1+b^{-2}\mu_0^2B^2)J_{hy}=(p_0+\Delta p)e\mu_{1h}\mathcal{E}_y - \mu_0^{-1}\mu_{1h}eDd(\Delta p)/dy, \quad (3.4)$$

where μ_0, μ_1, and μ_2 are quantities with the dimensions of mobility defined by

$$\mu_0\equiv(4/3\sqrt{\pi})\int_0^\infty \gamma x^{\frac{3}{2}}\exp(-x)dx\equiv(4/3\sqrt{\pi})I_0, \quad (3.5)$$

$$\mu_1\equiv(4/3\sqrt{\pi})(1+\mu_0^2B^2)\times\int_0^\infty\frac{\gamma x^{\frac{3}{2}}\exp(-x)}{1+\gamma^2B^2}dx\equiv(4/3\sqrt{\pi})(1+\mu_0^2B^2)I_1, \quad (3.6)$$

$$\mu_2^2\equiv(4/3\sqrt{\pi})(1+\mu_0^2B^2)\times\int_0^\infty\frac{\gamma^2x^{\frac{3}{2}}\exp(-x)}{1+\gamma^2B^2}dx\equiv(4/3\sqrt{\pi})(1+\mu_0^2B^2)I_2. \quad (3.7)$$

The hole quantities μ_{0h}, μ_{1h} and μ_{2h} are similarly defined. Since there is no continual accumulation of charge in

[10] A. H. Wilson, *Theory of Metals* (Cambridge University Press, New York, 1953), 2nd ed., p. 209 ff.
[11] H. Dember, Physik Z. 32, 554, 886 (1931); 33, 207 (1932).

the steady state

$$J_{ey}=-J_{hy}. \tag{3.8}$$

There is no bulk generation of excess carriers so that

$$d(J_{ey})/dy=-d(J_{hy})/dy$$
$$=e\Delta n/\tau_n(\Delta n)=e\Delta p/\tau_p(\Delta p), \tag{3.9}$$

and the boundary conditions are

$$[J_{ey}]_{y=0}=e\eta\phi-e\Delta n_0 S_n(\Delta n_0), \tag{3.10}$$

and

$$[J_{ey}]_{y=\infty}=0. \tag{3.11}$$

Equations (3.1) through (3.4) along with Eq. (3.9) are used to eliminate J_{hx}, J_{hy} and $\mathcal{E}_y$ to give

$$J_{ex}=-\mu_2^2\mu_1^{-1}BJ_{ey}, \tag{3.12}$$

$$J_{hx}=-\mu_{2h}^2\mu_{1h}^{-1}BJ_{ey}, \tag{3.13}$$

and

$$eD(d/dy)[(p_0+\Delta p)(n_0+\Delta n)]$$
$$=\mu_0\mu_1^{-1}[(p_0+\Delta p)(1+\mu_0^2B^2)$$
$$+\mu_1\mu_{1h}^{-1}(n_0+\Delta n)(1+b^{-2}\mu_0^2B^2)]J_{ey}. \tag{3.14}$$

The s-c current per unit sample width, given by

$$i_{sc}=\int_0^\infty (J_{ex}+J_{hx})dy,$$

becomes

$$i_{sc}=-(\mu_2^2/\mu_1+\mu_{2h}^2/\mu_{1h})eD\mu_1\mu_0^{-1}B$$
$$\times\int_0^\infty [(p_0+\Delta p)(1+\mu_0^2B^2)+\mu_1\mu_{1h}^{-1}(n_0+\Delta n)$$
$$\times(1+b^{-2}\mu_0^2B^2)]^{-1}\frac{d}{dy}[(p_0+\Delta p)(n_0+\Delta n)]dy$$

by the use of Eqs. (3.12)–(3.14). Since $p_0\gg\Delta p$, Δn, n_0, the denominator of the integrand is essentially constant so that the integral may be evaluated to give

$$i_{sc}=eDB\mu_1\mu_0^{-1}(\mu_2^2/\mu_1+\mu_{2h}^2/\mu_{1h})(1+\mu_0^2B^2)^{-1}$$
$$\times[1+(\Delta p/p_0)+(n_0\tau_p(\Delta p_0)/p_0\tau_n(\Delta n_0))]\Delta n_0. \tag{3.15}$$

For a strongly extrinsic p-type semiconductor

$$\Delta p/p_0+n_0\tau_p(\Delta p_0)/p_0\tau_n(\Delta n_0)\ll 1,$$

and since the ratio of electron effective mass to hole effective mass is much less than unity, the hole mobilities are negligible in comparison with the electron mobilities so that Eq. (3.15) may be simplified to

$$i_{sc}=e\mu_2^2\mu_0^{-1}BD(1+\mu_0^2B^2)^{-1}\Delta n_0. \tag{3.16}$$

When the ratio of excess holes to excess electrons is written as a function, $r(\Delta n)$, of excess electrons, Eq. (3.14) can be written as

$$\frac{d(\Delta n)}{dy}=\frac{\mu_0[(p_0+\Delta p)(1+\mu_0^2B^2)+b_1(n_0+\Delta n)(1+b^{-2}\mu_0^2B^2)]J_{ey}}{eD\mu_1[p_0+(n_0+2\Delta n)r(\Delta n)+(n_0+\Delta n)\Delta nr'(\Delta n)]}, \tag{3.17}$$

where $r'(\Delta n)=d[r(\Delta n)]/d(\Delta n)$ so that with the use of Eqs. (3.9) and (3.17)

$$J_{ey}\frac{dJ_{ey}}{d(\Delta n)}=\frac{e^2D\mu_1\Delta n[p_0+(n_0+2\Delta n)r(\Delta n)+(n_0+\Delta n)\Delta nr'(\Delta n)]}{\tau_n(\Delta n)\mu_0[(p_0+\Delta p)(1+\mu_0^2B^2)+b_1(n_0+\Delta n)(1+b^{-2}\mu_0^2B^2)]}. \tag{3.18}$$

Consequently

$$J_{ey}^2=2e^2D\mu_1\mu_0^{-1}(1+\mu_0^2B^2)^{-1}\int_0^{\Delta n}[1+p_0^{-1}(n_0+2\Delta n)r(\Delta n)+p_0^{-1}(n_0+\Delta n)\Delta nr'(\Delta n)]\frac{\Delta n}{\tau_n(\Delta n)}d(\Delta n) \tag{3.19}$$

for $p_0\gg\Delta p$, Δn, n_0. When Eq. (3.19) is applied to the boundary condition (3.10) the applied photon flux is related to the surface concentration of excess carriers by

$$K(B)f(\Delta n_0)=\eta\phi-\Delta n_0 S_n(\Delta n_0), \tag{3.20}$$

where

$$K(B)\equiv[2D\mu_1\mu_0^{-1}(1+\mu_0^2B^2)^{-1}]^{\frac{1}{2}}, \tag{3.21}$$

and

$$f(\Delta n_0)\equiv\left[\int_0^{\Delta n_0}(1+p_0^{-1}(n_0+2\Delta n)r(\Delta n)\right.$$
$$\left.+p_0^{-1}(n_0+\Delta n)\Delta nr'(\Delta n))\frac{\Delta n}{\tau_n(\Delta n)}d(\Delta n)\right]^{\frac{1}{2}}. \tag{3.22}$$

The evaluation of $\tau_n(\Delta n_0)$ is performed by noting that

$$[d/d(\Delta n_0)][f(\Delta n_0)]^2=\Delta n_0/\tau_n(\Delta n_0), \tag{3.23}$$

when

$$p_0^{-1}(n_0+2\Delta n_0)r(\Delta n_0)$$
$$+p_0^{-1}(n_0+\Delta n_0)\Delta n_0r'(\Delta n_0)\ll 1. \tag{3.24}$$

IV. METHOD OF ANALYSIS

A simple method of analysis of the experimental results may be used when the surface recombination velocity is negligible under all conditions. Equation (3.20) may then be written as

$$K(B)f(\Delta n_0)=\eta\phi. \tag{4.1}$$

When Eq. (4.1) is squared, differentiated with respect to Δn_0, and combined with Eqs. (3.16), (3.21), and

(3.23), the lifetime is given by

$$\tau_n(\Delta n_0)=\frac{\mu_1(1+\mu_0^2B^2)}{\mu_2^4B^2ekT\eta^2}\times\frac{i_{sc}}{\phi}\times\frac{di_{sc}}{d\phi}. \qquad (4.2)$$

Thus at constant magnetic field and varying photon flux, $(i_{sc}/\phi)(di_{sc}/d\phi)$ is proportional to $\tau_n(\Delta n_0)$, i_{sc} is proportional to Δn_0 [Eq. (3.16)], and a graph of $(i_{sc}/\phi)\times(di_{sc}/d\phi)$ against i_{sc} demonstrates the variation of $\tau_n(\Delta n)$ against Δn apart from constants of proportionality. These considerations may be used to provide a direct method of analysis.

Although the surface recombination velocity may be negligible in the small-signal region, it may not be negligible in the large-signal region. If, for instance, the "lifetime" were to increase with increasing Δn then $\phi/\Delta n_0$ would decrease with increasing Δn_0, and hence at the larger photon fluxes or larger magnetic fields $\phi/\Delta n_0$ may become comparable with $S_n(\Delta n_0)$, and the second term on the right-hand side of Eq. (3.20) would not be negligible.

A more general analysis applicable when the surface recombination velocity is negligible in the small-signal region only is now described. In order to calculate lifetime and surface recombination velocity from the theory developed in Sec. III, the mobilities μ_0, μ_1, and μ_2 must first be known. These quantities, which are determined from the magnetic field dependence of the s-c current in the small-signal region after a specific scattering mechanism has been assumed, are then used in the large-signal region to determine $\tau_n(\Delta n)$ and $S_n(\Delta n)$ as functions of Δn. Finally the self-consistency of these parameters is tested in the large-signal region to identify the scattering mechanism, since the analysis in the small-signal region is not sufficiently sensitive to distinguish between scattering mechanisms.

In the small-signal region, where τ_n is independent of excess carrier concentration and hence independent of photon flux and magnetic field, Eq. (4.2) may be

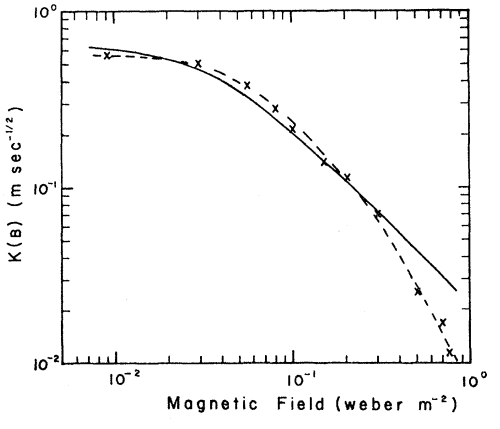

FIG. 6. A typical graph of $K(B)$ vs B [Eq. (3.21)] for an energy independent relaxation time. The dashed line is a least squares fit of $f^{-1}(\Delta n_0)[\eta\phi-\Delta n_0S_n(\Delta n_0)]$ with $K(B)$.

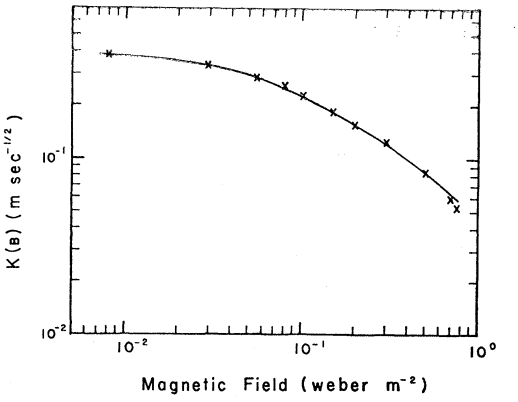

FIG. 7. A typical graph of $K(B)$ vs B [Eq. (3.21)] for ionized impurity type scattering. The crossed points are for a least squares fit of $f^{-1}(\Delta n_0)[\eta\phi-\Delta n_0S_n(\Delta n_0)]$ with $K(B)$.

solved for the s-c current to give

$$i_{sc}=\mu_2^2e\eta\phi D^{\frac{1}{2}}\tau_n^{\frac{1}{2}}B/\mu_0^{\frac{1}{2}}\mu_1^{\frac{1}{2}}(1+\mu_0^2B^2)^{\frac{1}{2}}, \qquad (4.3)$$

when there is negligible surface recombination velocity. This equation is in agreement with the result of others.[1–7] The magnetic field dependence of the theoretical s-c current in Eq. (4.3) is evaluated by using the definitions of μ_1 and μ_2 from Eqs. (3.6) and (3.7). In practice the relaxation time is taken to be related to the energy by a power law, so that $\gamma=Ax^m$, where A is a constant with dimensions of mobility and m is determined by the specific scattering mechanism assumed. Then the s-c current of Eq. (4.3) becomes a function of AB and may be written as

$$i_{sc}\propto BI_2/A^{\frac{1}{2}}I_1^{\frac{1}{2}}, \qquad (4.4)$$

where I_1 and I_2 are the integrals[12] defined in Eqs. (3.6) and (3.7). The right-hand side of (4.4), plotted as a function of AB, can then be compared to the experimental s-c current, plotted as a function of B for small constant photon flux, when both are plotted on log-log paper. The ordinates of the two graphs differ by the factor A which is thus determined. When A is known μ_0, μ_1, μ_2, and $K(B)$ may then be calculated using Eqs. (3.5)–(3.7) and (3.21).

The experimental data is taken in such a way that graphs of s-c current against photon flux at several constant magnetic fields may be plotted. A value for Δn_0 is chosen and the s-c current which would be required to give this surface concentration of excess electrons is calculated for each magnetic field according to Eq. (3.16). The value of photon flux, ϕ, which is required to produce this s-c current is found from the i_{sc} against ϕ curve appropriate to the magnetic field. Thus

[12] The integrals for $m=\frac{3}{2}$ were evaluated on an I.B.M. 704 digital computer over a greater range than can be obtained from tables; R. B. Dingle, D. Arndt and S. K. Roy, Appl. Sci. Research **B6**, 245 (1958). For $m=-\frac{1}{2}$ tabulated values were used; R. B. Dingle, D. Arndt and S. K. Roy, Appl. Sci. Research **B6**, 144 (1956).

for constant Δn_0, ϕ is known experimentally as a function of magnetic field, $K(B)$ is known theoretically, and in Eq. (3.20) $f(\Delta n_0)$ and $\Delta n_0 S_n(\Delta n_0)$ are unknown constants which may then be found by the method of least squares. This procedure is repeated for different values of Δn_0 which allows $\Delta n_0 S_n(\Delta n_0)$ and $f(\Delta n_0)$ to be plotted as functions of Δn_0.

The consistency of the values obtained is checked in two ways. First the quality of the least squares fit is examined for each constant Δn_0. Examples are shown in Figs. 6 and 7 and discussed in Sec. V. Second, $K^{-1}(B)[\eta\phi-\Delta n_0 S_n(\Delta n_0)]$ is calculated as a function of Δn_0 for each magnetic field with the use of the original experimental measurements and the derived graph of $\Delta n_0 S_n(\Delta n_0)$ vs Δn_0. The results for each magnetic field give the same curve which coincides with the graph of $f(\Delta n_0)$ vs Δn_0 determined by the least squares method, if the scattering mechanism originally assumed is the correct one.

Then knowing $f(\Delta n_0)$ as a function of Δn_0, $\tau_n(\Delta n)$ may be found from Eq. (3.23) as a function of Δn:

$$\tau_n(\Delta n_0)=\frac{\Delta n_0}{2f(\Delta n_0)}\frac{d(\Delta n_0)}{d[f(\Delta n_0)]}.$$

V. RESULTS

A. Mobility

The analysis of the experimental data by the method of Sec. IV requires that a scattering mechanism be initially assumed. Three cases were considered: (1) an energy-independent relaxation time, (2) acoustical lattice scattering[13] where $\tau_{\rm rel}\propto E^{-\frac{1}{2}}$, and (3) ionized impurity type scattering where it is taken that $\tau_{\rm rel}\propto E^{\frac{3}{2}}$. In the case of InSb at 80°K, the logarithmic term of the Conwell-Weisskopf treatment[14] of ionized impurity scattering, which is applicable here,[15] is found to be slowly varying and may be removed as a constant from the integrals of Eqs. (3.5)–(3.7).

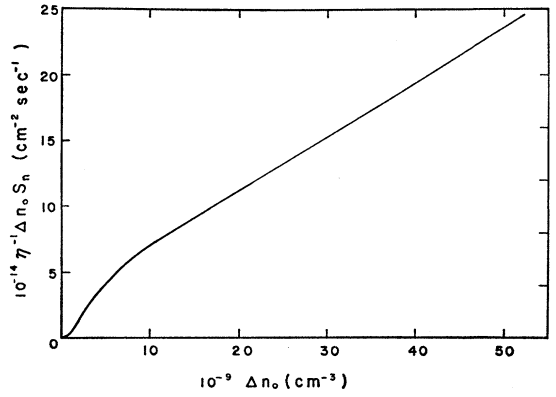

FIG. 8. Graph of $\eta^{-1}\Delta n_0 S_n(\Delta n_0)$ vs Δn_0 derived from the analysis of the experimental data when ionized impurity type scattering is assumed.

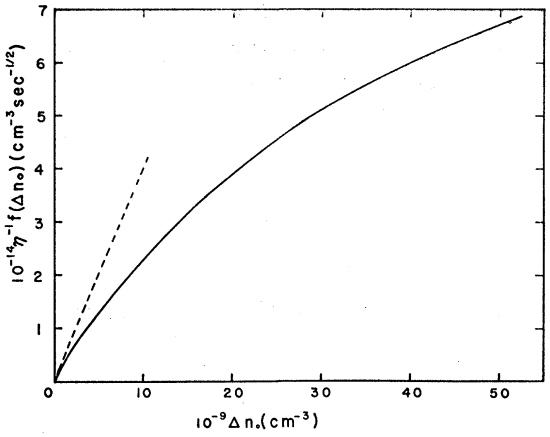

FIG. 9. Graph of $\eta^{-1}f(\Delta n_0)$ vs Δn_0 derived from the analysis of the experimental data when ionized impurity type scattering is assumed. The dashed line is a graph of $\eta^{-1}f(\Delta n_0)$ vs Δn_0 if the lifetime were constant at its small signal value.

Satisfactory agreement between theory and experiment was not obtained when an energy independent scattering mechanism was assumed. Figure 6 shows a typical least squares fit between theory and experiment for this case when the first consistency test of the analysis is applied. This poor agreement was anticipated in the discussion of Fig. 3. Lattice scattering proved to have better agreement in this respect but when the second consistency test was applied there was a spread of 20% which appeared to be systematic with magnetic field. The best agreement was obtained with ionized impurity type scattering for which a typical least squares fit is shown in Fig. 7. When the second test was applied the spread was completely random and no more than 5%. In this case the zero magnetic field mobility was found to be 1.1×10^5 cm^2/v-sec.

B. Surface Recombination Velocity and Lifetime

Since impurity type scattering gave the most consistent results, the ensuing discussion relates only to this mechanism. The functions $\Delta n_0 S_n(\Delta n_0)$ and $f(\Delta n_0)$ of Eq. (3.22) derived from the analysis are shown in Figs. 8 and 9. Figure 10 shows $S_n(\Delta n_0)$ as a function of Δn_0 derived from Fig. 8. The derivatives of $f(\Delta n_0)$ with respect to Δn_0 are determined from Fig. 9 and used in the last step of the analysis to determine the "lifetime" $\tau_n(\Delta n)$, as a function of Δn, which is shown in Fig. 11. The hole lifetime for our samples is of the order of 10^{-7} sec and is slowly varying in Δn so that r' may be taken as $-(\tau_p/\tau_n^2)(d\tau_n/d\Delta n)$. The maximum value which the left-hand side of the inequality (3.24) attains with $p_0\sim10^{14}$ cm^{-3} and $d\tau_n/d(\Delta n)$ determined from Fig. 11 is ~0.013 and may thus be neglected in comparison with unity.

[13] W. Shockley and J. Bardeen, Phys. Rev. **77**, 407 (1949); **80**, 72 (1950).

[14] E. Conwell and V. F. Weisskopf, Phys. Rev. **77**, 388 (1950).

[15] N. Sclar, Phys. Rev. **104**, 1548 (1956).

VI. CONCLUSION

The large-signal theory of Sec. III is in good agreement with experiment for p-type InSb at 80°K. As a consequence the dependence of lifetime and surface recombination velocity dependent on excess carrier concentration has been determined. It appears that scattering by ionized impurities is dominant, although the possibility of acoustical lattice scattering may not be ruled out entirely. The experimental results are not consistent with an energy-independent relaxation time contrary to the findings of others.[5,7] However, these previous conclusions were only based on the analysis of the small signal region where it is difficult to distinguish between different scattering mechanisms.

When PME measurements are made on semiconductors at low temperatures, the restrictions of small-signal theory necessarily mean the measurement of very small s-c currents. The ultimate sensitivity of the apparatus determines the smallest magnetic field which may be used for any particular photon flux. However, in the large-signal region, much smaller magnetic fields may be used giving increased accuracy in the measurement of the s-c current. A further advantage of the large-signal analysis is the increased information which it gives.

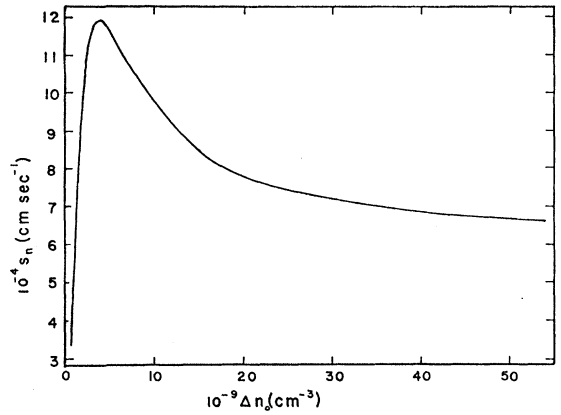

FIG. 10. Graph of electron "surface recombination velocity" vs Δn. A quantum efficiency of 1.4 was used in accord with J. Tauc [J. Phys. Chem. Solids 8, 219 (1959)].

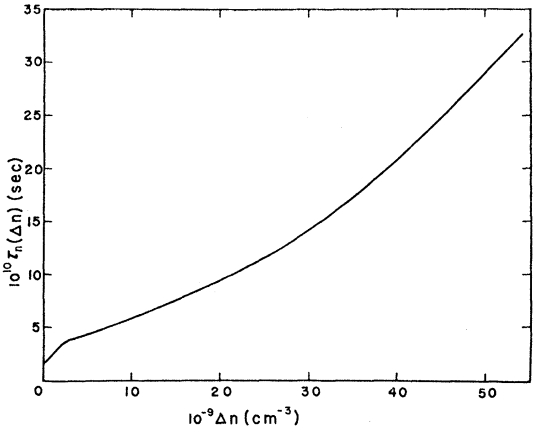

FIG. 11. Graph of electron "lifetime" vs Δn. A quantum efficiency of 1.4 was used.

At low temperatures the effect of background radiation can vastly alter results especially for small photon fluxes. It should also be noted that if the small-signal condition is assumed, reasonably small magnetic fields must be used even though a small photon flux is applied. The effect of increasing the magnetic field is to hold more carriers to the surface, thereby increasing the surface excess concentration.

ACKNOWLEDGMENTS

The authors wish to thank Mr. D. R. Powell for the computer programming, Mr. E. E. Harp for aid with the measurements, and Dr. W. M. Bullis for helpful discussions. We are also indebted to Dr. S. Parker for providing the various samples.